Low-lying states of ^{56}Fe

R. De Leo,[1,2] H. Akimune,[1] N. Blasi,[3] I. Daito,[1] Y. Fujita,[4] M. Fujiwara,[1] S. I. Hayakawa,[5] S. Hatori,[6] H. Ikegami,[1] T. Inomata,[1] I. Katayama,[1] K. Katori,[4] L. Lagamba,[2] S. Micheletti,[3] S. Morinobu,[1] R. Perrino,[8] M. Pignanelli,[3] H. Sakamoto,[9] J. Takamatsu,[7,*] and M. Tosaki[10]

[1]*Research Center for Nuclear Physics, Osaka University, Mihogaoka 10-1, Ibaraki 567, Osaka, Japan*
[2]*Dipartimento di Fisica dell'Universita' and Sezione INFN, via Amendola 173, I-70126 Bari, Italy*
[3]*Dipartimento di Fisica dell'Universita' and Sezione INFN, via Celoria 16, I-20133 Milano, Italy*
[4]*Department of Physics, Osaka University, Toyonaka 560 Osaka, Japan*
[5]*Ashikaga Institute of Technology, Ashikaga, Tochigi 326, Japan*
[6]*Department of Physics, Kyoto University, Sakyo, Kyoto 606, Japan*
[7]*Department of Physics, Tohoku University, Sendai 980, Japan*
[8]*Sezione INFN, via Arnesano, I-73100 Lecce, Italy*
[9]*Faculty of Engineering, Gifu University, Gifu 501-11, Japan*
[10]*Laboratory of Applied Physics, Kyoto Prefectural University, Kyoto 606, Japan*

(Received 10 September 1997)

Low-lying states at $E_x = 4.4-8.6$ MeV of excitation energy in ^{56}Fe have been studied by means of inelastic deuteron scattering at $E_d = 56$ MeV. The spin, parity, and isoscalar matrix element of detected levels have been deduced by comparing the measured cross sections with coupled-channel calculations using collective form factors. The present data for higher excitation energies have been analyzed by combining with previous data at lower excitation energies. The low-energy octupole strength in ^{56}Fe is found to be mostly located in the excitation energy range of $E_x = 4.4-8.6$ MeV. The strength is weakly fragmented, and the 3_1^- level exhausts the major part of the octupole energy-weighted-sum-rule value. A similar behavior is observed for the quadrupole strength in ^{56}Fe, which is mostly located below $E_x = 4.4$ MeV. This is in contrast with the behavior of the 3^- and 2^+ states in ^{54}Fe, which are heavily fragmented despite the weaker quadrupole deformation. The hexadecapole strength is strongly fragmented both in ^{56}Fe and in ^{54}Fe. The strength distributions for the transitions with multipolarities $\lambda = 2$, 3, and 4 in ^{54,56}Fe have been compared with random phase approximation calculations. The theoretical calculations show that the closure of the $\nu f_{7/2}$ shell is responsible for the observed fragmentation of the 2^+ and 3^- strengths in ^{54}Fe, and that the collectivity of the 2_1^+ and 3_1^- levels of ^{56}Fe is restored by the presence of two neutrons outside the $\nu f_{7/2}$ shell.
[S0556-2813(98)00504-4]

PACS number(s): 27.40.+z, 21.10.Hw, 21.10.Re, 25.45.De

I. INTRODUCTION

The strength distributions of low-order multipolarities are useful tools to test nuclear structure calculations. Recently, De Leo *et al.* [1] have studied the excited states in ^{56}Fe up to an excitation energy of 4.6 MeV through the inelastic scattering of deuterons and polarized protons. From a comparison with the γ-decay data, the neutron and proton transition matrices for the quadrupole excitations in ^{56}Fe have been deduced. These have been used to evidence the quadrupole mixed-symmetry (MS) [2] strength predicted by the neutron-proton interacting boson model (IBA-2) [3].

In this paper, we report on the isoscalar strength distribution for the octupole and the hexadecapole strengths, which lie at relatively high excitation energies in the same nucleus ^{56}Fe. As a probe to study these strengths, we use deuteron inelastic scattering at 56 MeV. Scattered particles have been detected by means of a magnetic spectrograph with a high-energy resolution. Many states in the excitation energies of ^{56}Fe between 4.4 and 8.6 MeV have been measured.

Experimental studies to detect the strength of the $\lambda = 2$, 3, and 4 multipolarities in other nuclei of the $A = 60$ region were performed [4–8] at the RCNP in the late 1980s. In particular, the fragmentation of the octupole strength was evidenced in four $N = 28$ isotones and three Ti isotopes.

In Ref. [4], the attention was focused on the one-particle–one-hole $(1p\text{-}1h)$ $[(\pi s_{1/2})^{-1}(\pi f_{7/2})]$ nature of the 3_1^- level of the ^{48}Ca, ^{50}Ti, ^{52}Cr, and ^{54}Fe isotones. Fujiwara *et al.* have shown that its strength exhausts a fraction of the octupole energy-weighted sum rule (EWSR) which scales nearly as the unoccupancy probabilities of the $\pi f_{7/2}$ orbit (8:6:4:2). The fragmentation of the octupole strength in ^{46,48,50}Ti is found [5] to increase in going from spherical ^{50}Ti to deformed ^{46}Ti, and thus to be proportional to the nuclear quadrupole deformation parameter β_2. A similar correlation between octupole fragmentation and β_2 has been found for Mo, Pd, and Cd isotopes by Pignanelli *et al.* [9]; the octupole fragmentation in Mo, Pd, and Cd is interpreted in terms of the IBA model, and is inferred to be induced by the quadrupole-octupole interaction.

Recently, octupole fragmentation has been evidenced in many other nuclei and a review of the effect has been reported in Refs. [10,11]. Cottle *et al.* [10] have clearly shown

*Present address: Toshiba ULSI Laboratory, Kawasaki 210, Japan.

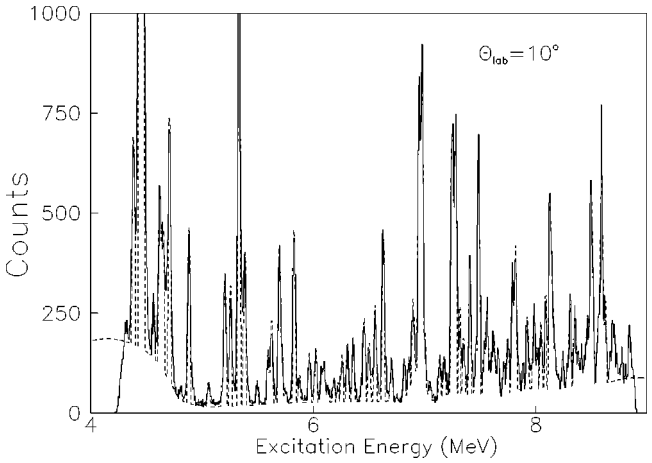

FIG. 1. Energy spectrum (shown as the solid line) for the inelastic scattering of 56 MeV deuterons at the scattering angles of 10°. The dashed histogram is a fit to the experimental data.

that the correlation between octupole fragmentation and β_2 is generally weak. In fact, with only a few exceptions, all the octupole strengths in nuclei with the mass $A>60$ are found to have a fragmentation (ΔE_3) widely distributed with β_2, although all are below the delimiting line $\Delta E_3=(\beta_2+0.1)$ MeV.

The study of the hexadecapole strength and of its fragmentation [12,13] is more complex due to the mixing of the hexadecapole vibration with the two-phonon quadrupole-quadrupole configuration.

The main purpose of this paper is to compare the $\lambda=2$, 3, and 4 strength distributions of ^{54,56}Fe. We find that the $\lambda=2$ and 3 strengths are fragmented only in ^{54}Fe, while the $\lambda=4$ one is fragmented in both nuclei. From a comparison of the experimental strengths with random phase approximation (RPA) calculations, we show that the $\lambda=2$ and 3 fragmentation in ^{54}Fe is strongly associated with the closure of the $\nu f_{7/2}$ shell, and that collectivity of these two multipolarities in ^{56}Fe is restored by the presence of the two neutrons outside the $f_{7/2}$ shell.

II. EXPERIMENTAL METHOD AND RESULTS

The inelastic scattering experiment was performed at the Research Center for Nuclear Physics (RCNP) in Osaka. Only a short description of the experimental apparatus is reported here since the details have been described in Ref. [1].

A beam of 56 MeV unpolarized deuterons was extracted from the AVF cyclotron with an intensity of about 60 nA. The target used was a self-supporting ^{56}Fe foil with a thickness of 1.05 mg/cm^2 and with an isotopic enrichment greater than 99%. Scattered deuterons were detected by using the magnetic spectrograph ''Raiden'' [14] with a solid angle of 3.2 msr. The magnetic field setting of the spectrograph covered the range of excitation energies from 4.4 to 8.6 MeV. The kinematic line broadening of the scattered deuterons was compensated by adjusting the multipole field of the spectrograph. A final energy resolution of about 30 keV full width at half maximum (FWHM) was obtained. An example of the obtained energy spectra is shown in Fig. 1. The area and location of each peak and background distribution were determined by using a peak fitting program (dashed line in Fig. 1). Energy spectra were measured in the angular range of $\theta_{\rm lab}=10°-50°$ in steps of 2.5°.

The excitation energy of the ^{56}Fe levels is listed in the third column of Table I. Previous data for levels below $E_x=4.45$ MeV from Ref. [1] are also listed. The first two columns of Table I show excitation energies and the spin values cited from the compilation data for ^{56}Fe given in Ref. [15]. Not all the levels listed in this compilation data have been resolved in the present experiment, while several new levels have been detected above 7 MeV.

The excitation energies of the detected levels, listed in the third column of Table I, were obtained by averaging the values from the calibrated spectra at all the explored scattering angles. An overall uncertainty is estimated to be 3 keV in the quoted energies below 7.5 MeV, and 8 keV at higher excitation energies due to the lack of levels for energy calibration.

The yield of each peak in the spectra was converted into cross sections by using the information on the target thickness, the solid angle, and the collected charges. The systematical uncertainty for the experimental cross sections has been estimated to be of the order of 10%. Measured cross sections for some strongly excited states are presented in Figs. 2–5. The error bars on the data points in the figures represent only the statistical error.

III. DATA ANALYSIS

Spin and parities (J^π) of the states excited by inelastic scattering can be inferred from the transferred angular momentum λ, deduced from a comparison between experimental and calculated differential cross sections. For this purpose, coupled-channel calculations have been carried out using the code ECIS88 [16]. Optical model parameters used in the present analyses are given in Table I of Ref. [1]. The first-derivative form factors are applied for the $\lambda\geqslant 2$ transitions. For $\lambda=0$ and 1, the form factors were evaluated on the basis of the work in Ref. [9]. Only direct $0^+_{\rm g.s.}$-J^π excitations were included in the calculation of the cross sections. They showed a marked difference in the angular shape for different transferred angular momentum, as shown in Figs. 2–4 for a λ transfer of 2, 3, and 4, respectively. For many levels, the J^π assignment was possible without any uncertainty. The results are listed in the fourth column of Table I without parentheses.

For states unresolved from neighbors (doublets), the assignment was tried with an incoherent sum of two transferred angular momenta. For states of weak intensity or with an angular distribution badly reproduced by the calculations, the J^π determination was doubtful. It was not possible in the worst cases. Examples of these cases are reported in Fig. 5. Tentative assignments of J^π are shown in the fourth column of Table I.

The coupling constants (β_λ) of the direct $0^+_{\rm g.s.}$-J^π excitations, obtained from a fit of calculated and experimental cross sections, are listed in fifth column of Table I.

The transition matrix elements are derived from the β coupling constants by using the following expression:

TABLE I. Energy and spin parity of ^{56}Fe excited levels from Ref. [15] (first two columns, labeled NDS) and from the present ^{56}Fe(d,d') experiment taken at $E_d=56$ MeV (fourth and fifth columns). The deformation parameters, the reduced matrix elements, and the EWSR percentages, deduced from the analyses described in the text, are reported in the last columns. The data in the last five columns and up to the $E_x=4510$ line have been taken from Ref. [1].

E_x(NDS) (keV)	J^π(NDS)	E_x(expt) (keV)	J^π	β_λ	$M(E\lambda)$ (e fm$^\lambda$)	EWSR (%)
846	2^+	846	2^+	0.183	36.2	4.6
2085	4^+	2085	4^+	0.023	214	0.04
2657	2^+	2657	2^+	0.040	8.0	0.71
2959.8	2^+	2960	2^+	0.006	1.2	0.02
3122.9	4^+	3123	4^+	0.053	492	0.34
3369.7	2^+	3370	2^+	0.031	6.1	0.52
3601.8	2^+	3602	2^+	0.028	5.5	0.46
3830.3	2^+	3832	2^+	0.021	4.1	0.27
4100.2	4^+	4100	4^+	0.036	334	0.21
4298	4^+	4298	4^+	0.019	173	0.06
4400.8	2^+	4400	(2^+)	0.013	2.6	0.12
4458	4^+	4459	4^+	0.039	359	0.26
4510	3^-	4510	3^-	0.118	155	4.85
4539	$1^+,2^+$	4539	(3^-)	0.045	58.6	0.69
4544						
4554	$2^+,3^+,4^+$	4554	(3^-)	0.024	31	0.37
4558						
4602						
4612	4^+	4612	4^+	0.017	155	0.05
4660	$2^+,3^+,4^+$	4660	4^+	0.023	210	0.09
4675						
4684	4^+	4684	4^+	0.015	135.5	0.04
4697						
4700	7^+					
4721						
4729	2^+	4729	2^+	0.023	4.47	0.4
4730	0+					
4739	$2^+,3^+,4^+$					
4802						
4822		4822	7^-	0.0126		
4847						
4868						
4877	4^+					
4878	2^+	4878	8^+	0.04		
4881						
4885						
5023						
5027		5027	2^+	0.008	1.52	0.049
5041	4^+					
5062						
5122	5^-					
5133						
5143		5143				
5148						
		5161	4^+	0.03	276	0.18
5186	1^-					
5188	2^+	5188	3^-	0.0255	33.4	0.26
5219						
5227	1					
5231	(2^+)					
5240						

TABLE I. (*Continued*).

E_x(NDS) (keV)	J^π(NDS)	E_x(expt) (keV)	J^π	β_λ	$M(E\lambda)$ (e fm$^\lambda$)	EWSR (%)
5249	4^+					
5256	8^+					
5257	2	5257	2^+	0.032	6.36	0.89
5274						
5296	0^+					
5306		5306	4^+	0.029	271	0.176
5386	0^+					
		5399	2^+	0.0075	1.48	0.049
5402	0					
5444						
5476	0^+					
5490		5490	(2^+)	0.009	1.72	0.07
				(8^+)	0.016	
5503						
5512	2^+	5512	2^+	0.014	2.79	0.18
5528						
5557						
5577	2^+	5577	2^+	0.017	3.42	0.27
		5600	2^+	0.011	2.15	0.11
5612						
5621						
		5625	4^+	0.008	75.15	0.014
5627	8^+					
5663						
5673						
5684						
		5695	2^+	0.019	3.76	0.336
5707						
5725						
5737		5737	2^+	0.008	1.52	0.055
5768	(4^+)					
5795						
5813		5813	4^+	0.0145	134.5	0.047
5824						
5853						
5863	4^+	5863	2^+	0.014	2.79	0.19
5869						
5874						
5882						
5908		5908	5^-	0.016		
5921						
5932	2^+	5932	2^+	0.012	2.42	0.145
5941						
5962		5962	2^+	0.006	1.24	0.038
5984						
6002						
6013		6013	2^+	0.006	1.24	0.038
6024						
6030						
6045						
6052	2^+	6052	$(2^+,3^-)$			
		6060	2^+	0.008	1.53	0.059
6071	6^+					
6078						

TABLE I. (*Continued*).

E_x(NDS) (keV)	J^π(NDS)	E_x(expt) (keV)	J^π	β_λ	$M(E\lambda)$ (e fm$^\lambda$)	EWSR (%)
6092	(3^-)	6092	2^+	0.009	1.77	0.08
6110	(0^+)					
6116	9					
		6129	(2^+)	0.009	1.77	0.08
			(4^+)	0.008	71.9	0.014
6138						
6174		6174	2^+	0.011	2.1	0.11
6201						
6219						
6250	1	6250	4^+	0.014	131	0.048
6265	4^+	6265	(2^+)	0.011	2.15	0.121
			(4^+)	0.011	102	0.029
6289						
6307						
6316		6316	2^+	0.01	1.98	0.103
6327						
6351						
6363		6363	(2^+)	0.0115	2.27	0.137
			(3^-)	0.012	15.9	0.071
6382						
6397						
6432		6432	2^+	0.02	3.95	0.42
6450						
6463		6463	(2^+)	0.01	2.16	0.23
6489	(2^+)					
6509		6509	2^+	0.009	1.76	0.084
6527						
6543		6543	(3^-)	0.004		
6555						
6563	0^+					
6593						
6613		6613				
6630						
6652						
6662	3^-	6662				
6670						
6698	1	6698				
6700						
6709						
6725						
6742		6742	3^-	0.028	37.07	0.41
6767						
6781	3^-	6781	3^-	0.028	37.07	0.41
6800	0^+	6800				
6815						
6843						
6856		6856	6^+	0.009		
6878	(3^-)					
6916						
6926	1					
6940		6940	2^+	0.0084	1.66	0.08
6967						
6979		6979	2^+	0.008	1.60	0.075
6994						

TABLE I. (*Continued*).

E_x(NDS) (keV)	J^π(NDS)	E_x(expt) (keV)	J^π	β_λ	$M(E\lambda)$ (e fm$^\lambda$)	EWSR (%)
7013		7013				
7036						
7055		7055	3^-	0.023	30.26	0.29
7066	1^+					
7077						
7085						
7090		7090	3^-	0.0225	29.47	0.27
7102						
7124	0^+					
7135	1	7135	3^-	0.0130	17	0.1
7154						
7167	1	7167	2^+	0.010	2.0	0.12
7170						
7189						
7204						
7211	1					
7220	0^+	7220	2^+	0.015	2.93	0.26
7248						
7283		7283	3^-	0.0122	15.98	0.083
7290	0^+					
7312		7312	(2^+)	0.019	3.70	0.42
		7355	2^+	0.009	1.76	0.095
7380		7380	(0^+)	0.0045		
		7412	3^-	0.01	12.6	0.052
7420						
7446	1	7446	(2^+)	0.0084	1.66	0.086
			(3^-)	0.0076	9.96	0.033
7468						
7475	(3^-)	7475				
		7489	2^+	0.008	1.59	0.079
		7543	2^+	0.0073	1.44	0.065
7580						
		7582	(2^+)	0.0095	1.88	0.11
			(4^+)	0.01	91	0.03
		7626	(2^+)	0.0104	2.06	0.135
			(3^-)	0.0105	13.76	0.064
7630						
		7658	(2^+)	0.011	2.15	0.148
			(3^-)	0.0122	15.98	0.087
7670						
7720						
		7731	2^+	0.007	1.34	0.058
		7776	2^+	0.01	1.98	0.127
7780						
7840		7841	2^+	0.0114	2.25	0.166
7870	2^+					
		7877	6^+	0.0192		
7887						
		7915	(5^-)	0.0095		
		7956	(2^+)	0.009	1.78	0.105
			(3^-)	0.0122	15.98	0.09
		8002	3^-	0.019	24.5	0.215
		8017	2^+	0.0114	2.25	0.17
		8036				

TABLE I. (*Continued*).

E_x(NDS) (keV)	J^π(NDS)	E_x(expt) (keV)	J^π	β_λ	$M(E\lambda)$ (e fm$^\lambda$)	EWSR (%)
8050						
		8075				
8110	0^+					
8120	2^+					
8128	1					
		8132	(2^+)	0.009	1.76	0.106
		8177	(4^+)	0.009	82.57	0.025
		8209	3^-	0.0122	15.98	0.094
8220						
8239	1					
		8258	3^-	0.012	15.46	0.088
		8292	(1^-)	0.071		
8307						
		8327	5^-	0.01		
		8362	(5^-)	0.01		
		8380	(3^-)	0.0113	14.8	0.082
		8426	(3^-)	0.0164	21.45	0.17
		8449	2^+	0.011	2.15	0.164
		8483	3^-	0.0122	15.98	0.097
		8516	3^-	0.0135	17.68	0.12
8536	1					
		8542	4^+	0.02	185.56	0.13
		8580	(3^-)	0.0127	16.64	0.106

$$M(E\lambda)=\frac{A}{2}\beta_\lambda\frac{\int V_{\rm tr}(r)r^\lambda d\tau}{\int V(r)d\tau}, \tag{1}$$

where $V_{\rm tr}(r)$ and $V(r)$ refer to the transition and central potentials, respectively. The derived matrix elements are given in the sixth column of Table I. These matrix elements are isoscalar (M_S) since they are derived from inelastic deuteron scattering.

The reduced transition probabilities and the matrix elements have a relation of

$$B(E\lambda,J_i\rightarrow J_f)=\frac{|M(E\lambda)|^2}{(2J_i+1)}. \tag{2}$$

Following Ref. [9], the EWSR for $\lambda\geqslant 2$ is

$$S_\lambda=\frac{\hbar^2}{8m\pi}\lambda(2\lambda+1)^2\frac{A}{4}\langle r^{2\lambda-2}\rangle, \tag{3}$$

with the $\langle r^{2\lambda-2}\rangle$ radii evaluated only from the real potential. The EWSR fractions obtained are reported in the last column of Table I for the $J^\pi=2^+$, 3^-, and 4^+ levels.

The estimated average error on β's and M's (not quoted in Table I) is around 10%. The error due to data analysis is usually larger than statistical and systematical ones. This is especially true for the levels excited with the strong couplings through the strongly excited 2_1^+ or 3_1^- levels. The error is negligible only in the few cases of very good fits to the experiment.

For some transitions observed in this work, a measurement of the isovector part of the transition matrix elements is available in the literature. For ^{56}Fe, these have been deduced in Ref. [1] through a comparison of (p,p'), (d,d') and γ-decay experiments. Both for ^{56}Fe and for ^{54}Fe, similar data are available from the inelastic scattering of π^+ and π^- in Ref. [17]. In Figs. 6 and 7, the available isoscalar and isovector transition matrix elements for the $\lambda=2$, 3, and 4 multipolarities are reported for ^{54}Fe and ^{56}Fe, respectively. The sign of the isovector elements is relative to that of the isoscalar ones.

Some features of a strength distribution are better seen by plotting its energy cumulative sum. This is shown in Fig. 8 for the isoscalar strengths (solid lines) of ^{54}Fe (left side) and ^{56}Fe (right side). The summed values for the $\lambda=2$, 3, and 4 multipolarities are shown in the upper, central, and lower parts in Fig. 8, respectively. The fragmentation of the $\lambda=2$ and 3 strengths is larger in the case of ^{54}Fe compared to that of ^{56}Fe.

IV. ISOSCALAR STRENGTH FRAGMENTATION

Recently a parametrization of the octupole fragmentation was given in Refs. [10,11]. By defining the centroid of the strength as

$$C_3=\frac{\sum_i E_i B(E3,0^+_{\rm g.s.}\rightarrow 3^-_i)}{\sum_i B(E3,0^+_{\rm g.s.}\rightarrow 3^-_i)}, \tag{4}$$

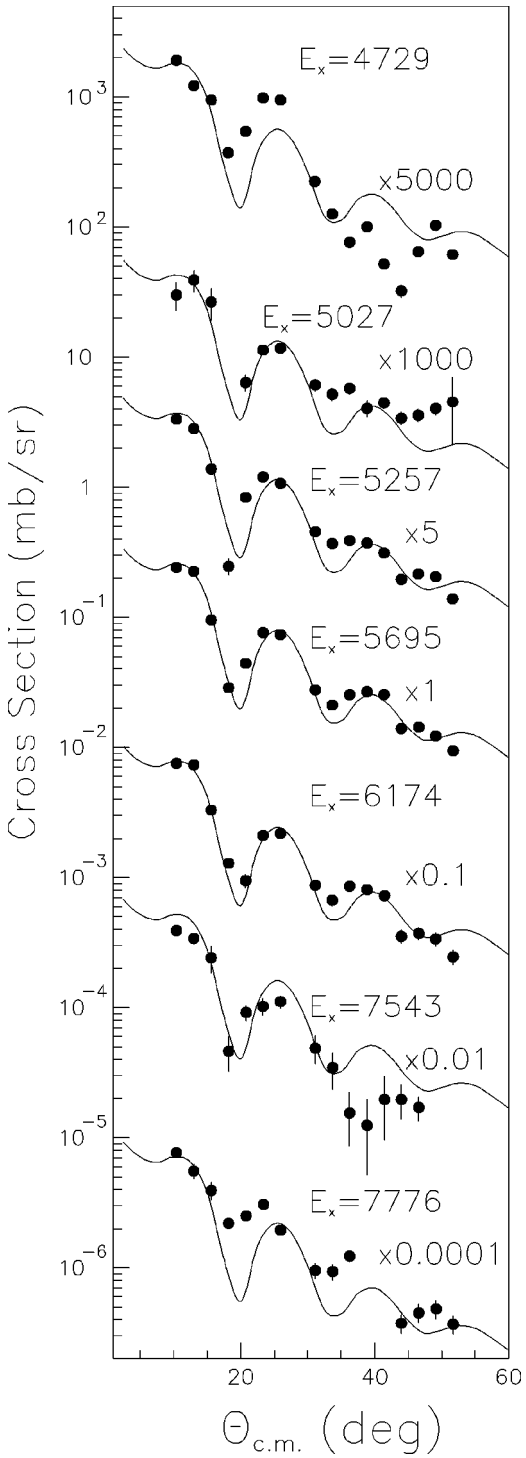

FIG. 2. Differential cross section for selected 2^+ states in ^{56}Fe from deuteron inelastic scattering at 56 MeV. The experimental data are shown by the solid circles. The excitation energies (E_x) of the selected states are indicated in keV. The curves are the results from coupled-channel calculations. Experimental data and the results of calculations have been multiplied by the factors indicated in the figure.

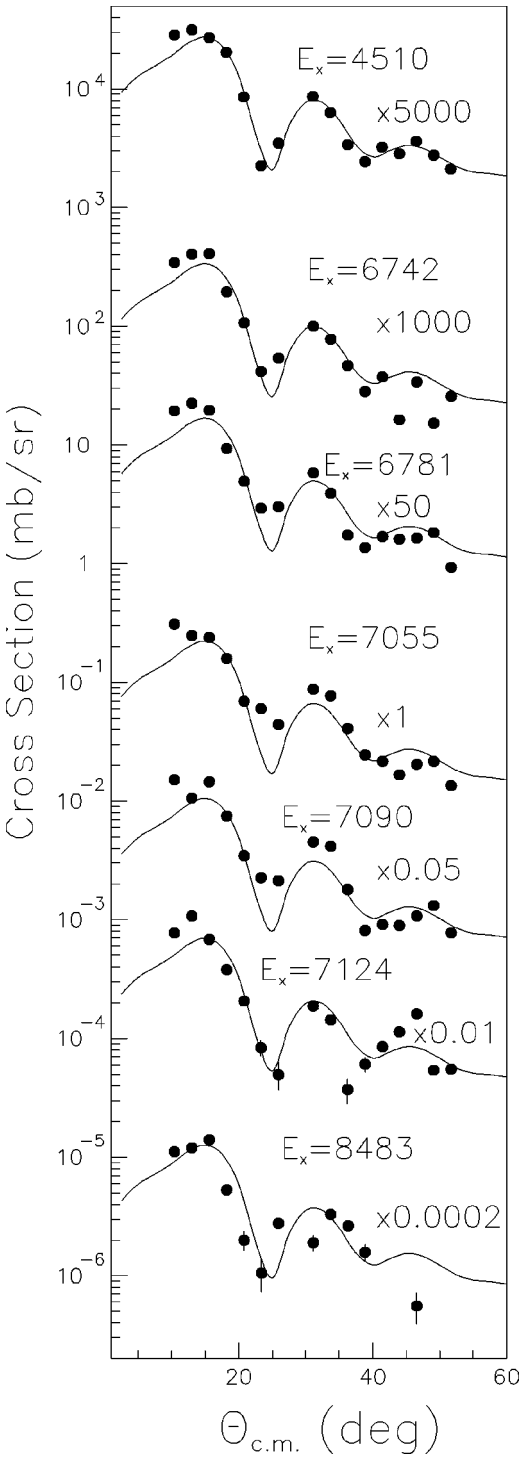

FIG. 3. Same as Fig. 2 for selected $J^\pi=3^-$ excited levels of ^{56}Fe.

a measure of the fragmentation is defined as

$$\Delta E_3 = C_3 - E(3_1^-). \tag{5}$$

In the present work, we adopt Eqs. (4) and (5) to parametrize the fragmentation of the low-lying strength, and we extend these definitions also to the $\lambda=2$ and 4 multipolarities.

A crucial point in Eq. (4) is the number of states involved in the sum or, equivalently, the interval of excitation energy spanned. To measure the octupole fragmentation due to the quadrupole-octupole interaction, the sum is generally extended to only four 3_K^- states which correspond to the different alignments of the octupole phonon ($K=0$, 1, 2, and 3) with respect to the symmetry axis of the nucleus.

Some difficulties are encountered in the individuation of these states since many experiments do not determine the K quantum number. The 3^- states deriving from the K frag-

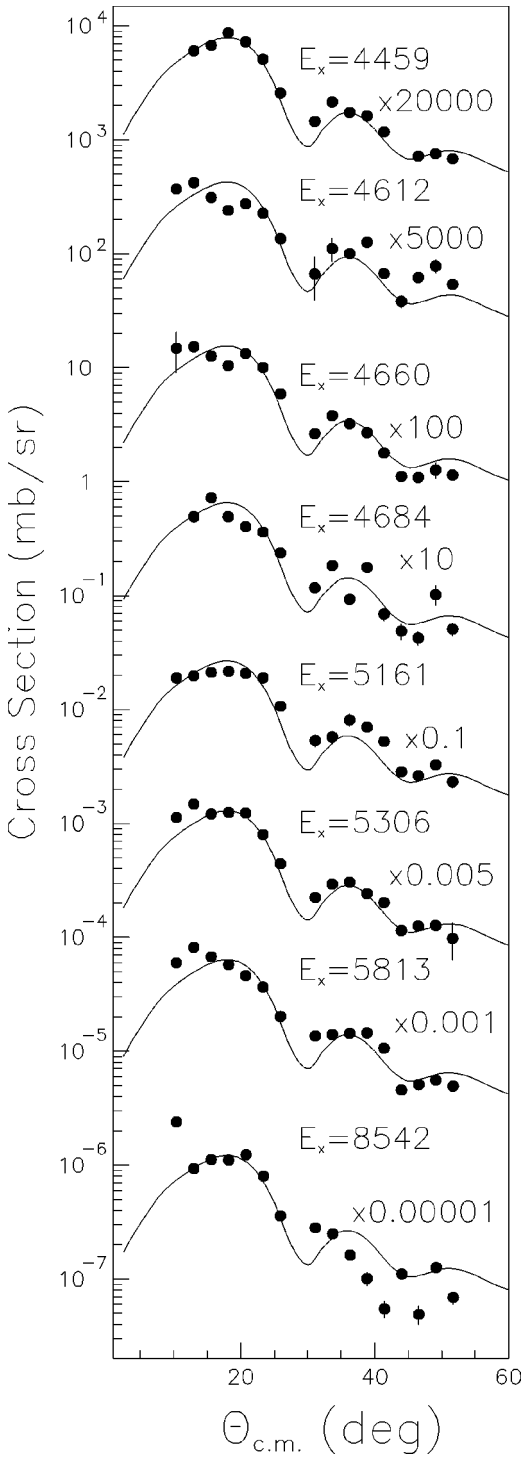

FIG. 4. Same as Fig. 2 for selected $J^{\pi}=4^{+}$ excited levels of ^{56}Fe.

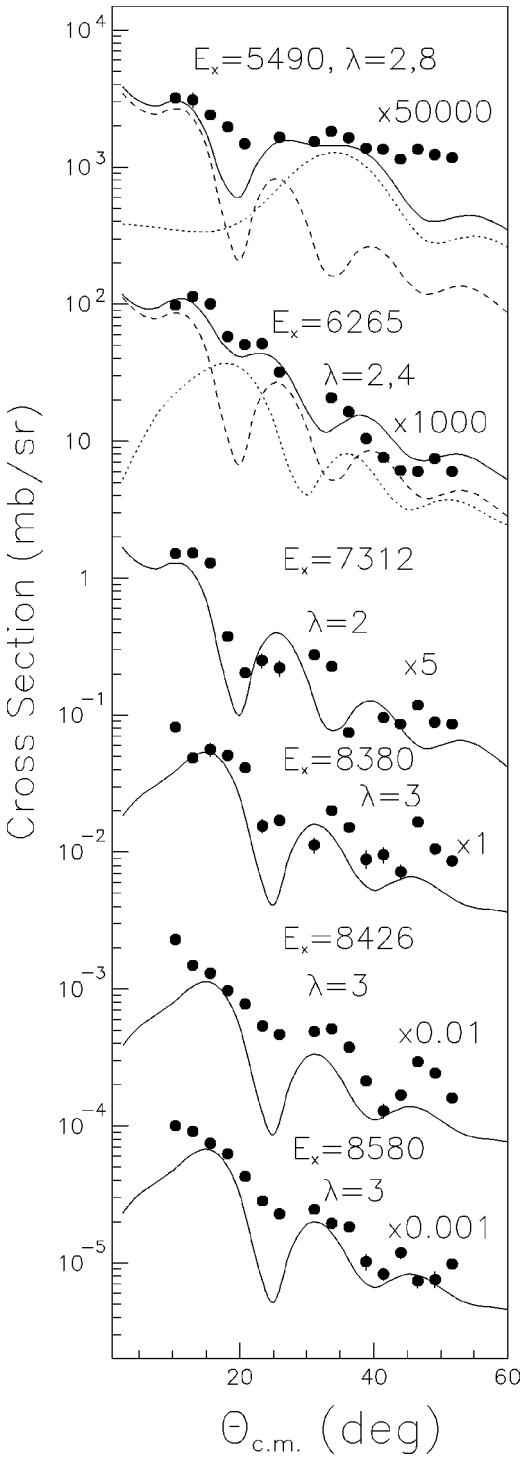

FIG. 5. Same as Fig. 2 for selected excited levels of ^{56}Fe whose attribution of J^{π} is uncertain. In some cases, the fit (solid curves) has been tried considering the level as an unresolved doublet with the indicated multipolarities and with contributions shown by the dashed and dotted curves.

mentation of the 3_1^- level are often split and mixed with 3^- states of a different nature. For this reason, the most intense 3^- states have been selected [7] to measure the fragmentation.

Moreover, in the mass region below $A=60$, the centroids of the low-energy octupole resonance (LEOR) expected at $E_x=30A^{-1/3}$ MeV approach the energies of the low-lying octupole states. To avoid the inclusion of contributions from the states in the LEOR, the octupole fragmentation data available in the literature are limited to nuclei with $A>60$ in the review in Refs. [10,11]. With only a few exceptions, Cottle *et al.* [10] found that all the ΔE_3 values are widely distributed below the delimiting $\Delta E_3=(\beta_2+0.1)$ MeV line (reported as a solid line in Fig. 9). Zamfir *et al.* [11] instead examined the octupole fragmentations in the contest of the sd-f approximation of the interacting boson model (IBA-f), and predicted that the largest fragmentations occur for nuclei in the O(6)→SU(3) transition region, and that

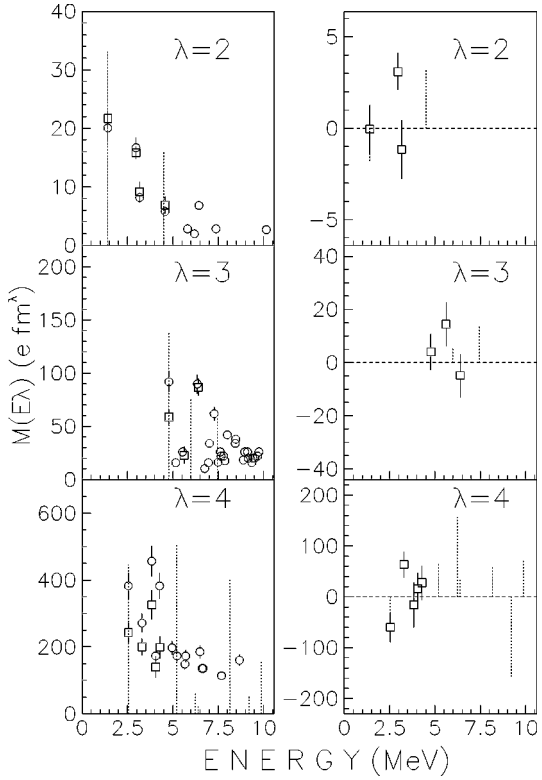

FIG. 6. The $\lambda=2$, 3, and 4 isoscalar (left part) and isovector (right part) matrix elements of ^{54}Fe. Values from Ref. [4] are reported with dots, values from Ref. [17] with squares. Vertical dotted lines are the results of the RPA calculations described in the text.

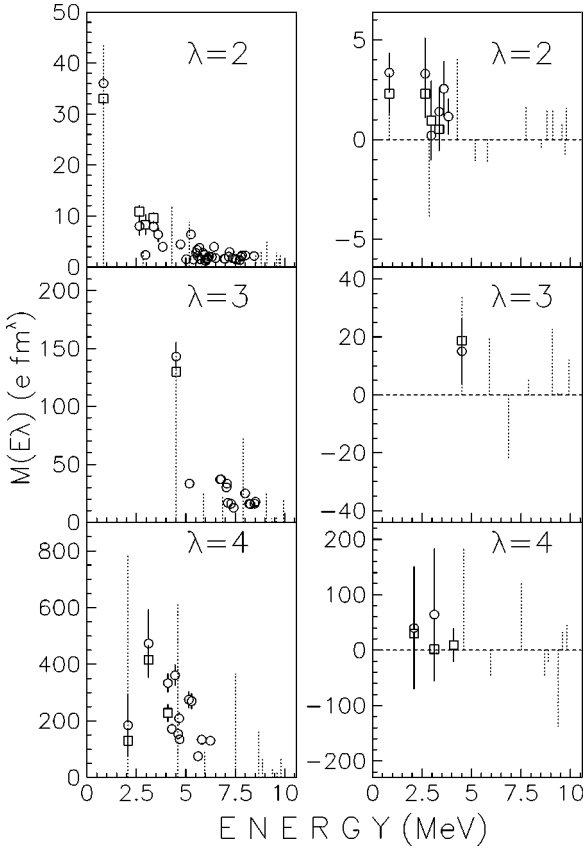

FIG. 7. The $\lambda=2$, 3, and 4 isoscalar (left part) and isovector (right part) matrix elements of ^{56}Fe. Values from this paper and from Ref. [1] are reported with dots, values from Ref. [17] with squares. Vertical dotted lines are the results of the RPA calculations described in the text.

the experimental values are distributed below this limit with a few exceptions. This limit for IBA-f octupole fragmentation is shown as a dashed line in Fig. 9.

The experimental points in Fig. 9 represent the fragmentations of the $\lambda=2$, 3, and 4 isoscalar strengths deduced for the levels in ^{56}Fe deduced from the present work, and taken from Refs. [4–8] for the other $A<60$ nuclei. Open circles, squares, triangles, stars, and crosses refer to the data for Ti, Fe, Ca, Cr, and Ni isotopes, respectively. The energy limits used in the sum of Eq. (4) are reported in Table II for the investigated nuclei. The fragmentations are displayed in three different ways to show their systematical trend. These are plotted as a function of the neutron number N (in the left side of Fig. 9), the quadrupole deformation parameter β_2 (in the central part), and the $R_{4/2}$ parameter defined as the ratio between the excitation energies of the 4_1^+ and 2_1^+ levels (in the right part).

We observe that the fragmentation values generally increase with increasing the multipolarity. Their averages are 0.9, 1.4, and 2 MeV for the $\lambda=2$, 3, and 4 multipolarities, respectively. This denotes that higher multipolarities are more fragmented.

Moreover, it is clear at least for ΔE_2 and ΔE_3 that the fragmentation values decrease with increasing the parameters β_2 and $R_{4/2}$, which are a measure of the collectivity of the nucleus. ^{56}Fe has the lowest octupole fragmentation. All the other nuclei have higher ΔE_3 values, well above the limiting lines of Refs. [10,11].

In order to disentangle the LEOR contributions from the octupole fragmentations, the ΔE_3 values have been reevaluated by limiting the sum in Eq. (4) to the four most intense 3^- states. These new values, which are reported as solid symbols in the central part of Fig. 9, are obviously lower than the open symbols. They, however, still decrease with β_2

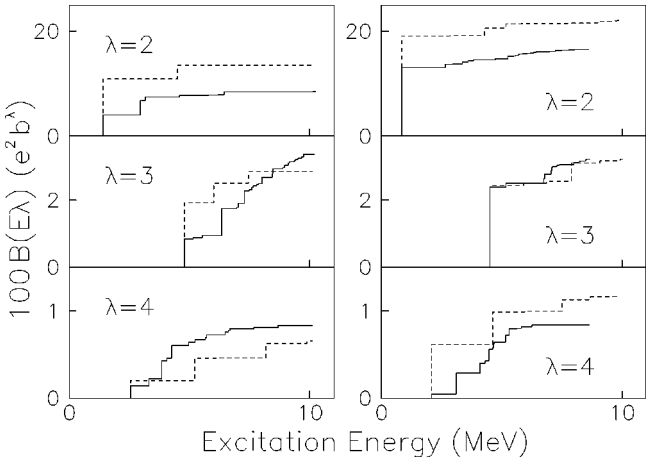

FIG. 8. Cumulative sums of the isoscalar strengths (solid lines) of ^{54}Fe (left side) and of ^{56}Fe (right side). The $\lambda=2$, 3, and 4 values are displayed in the upper, central, and lower parts of the figure, respectively. Dashed lines are the results from the RPA calculations described in the text.

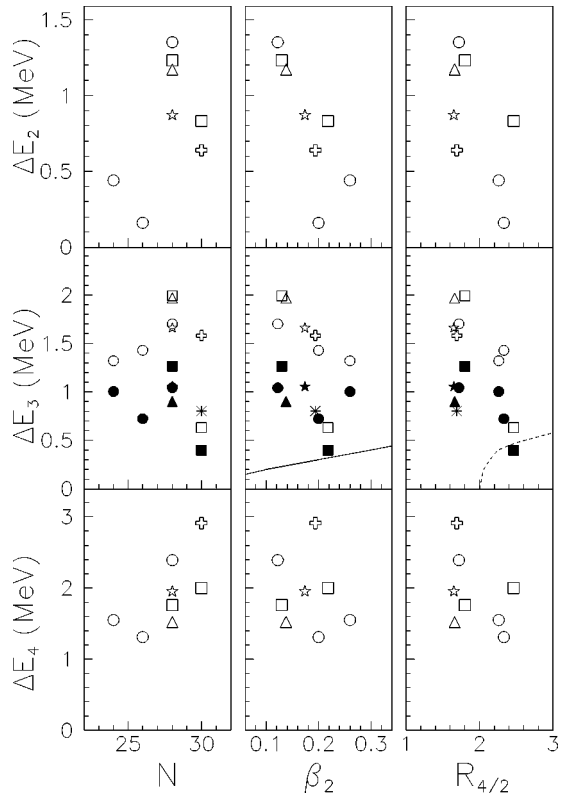

FIG. 9. Fragmentations, as defined in Eq. (4), of the quadrupole (ΔE_2), octupole (ΔE_3), and hexadecapole (ΔE_4) strengths versus the neutron number N (left side), the quadrupole deformation parameter β_2 (central part), and the $R_{4/2}$ (right side) parameter defined as the ratio between the excitation energies of the 4_1^+ and 2_1^+ levels. Open symbols refer to values evaluated with the sum in Eq. (4) extended up to the energies listed in Table II, solid symbols to values in which the sum in Eq. (4) is restricted to only the four most intense octupole levels. Circles, squares, triangles, stars, and crosses refer to Ti, Fe, Ca, Cr, and Ni isotopes, respectively. The solid line is taken from Ref. [10], the dashed curve from Ref. [11].

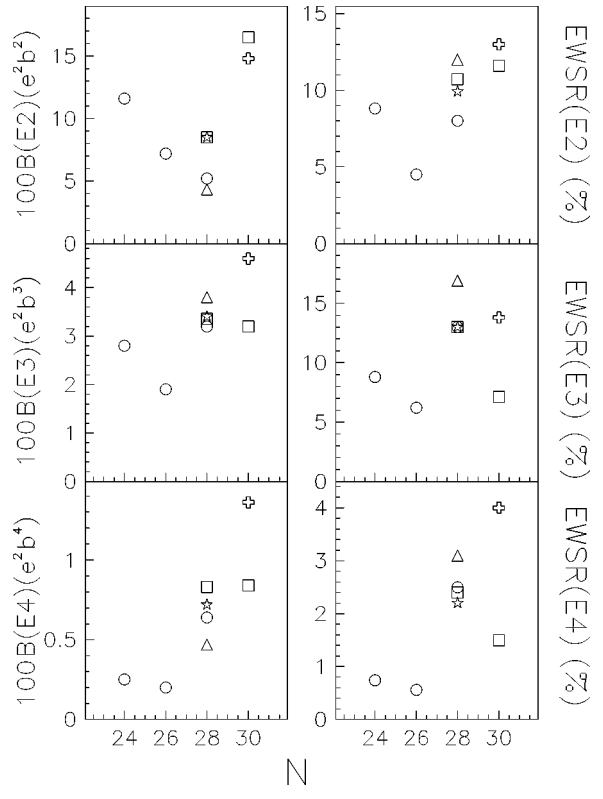

FIG. 10. The isoscalar $\lambda=2$, 3, and 4 total strengths (left part) and observed percentages of the sum rules (right part) displayed versus the neutron number N. The values refer to the energy limits listed in Table II. The $\lambda=2$, 3, and 4 multipolarity values are displayed in the upper, central, and lower parts of the figure, respectively. Circles, squares, triangles, stars, and crosses refer to Ti, Fe, Ca, Cr, and Ni isotopes, respectively.

and $R_{4/2}$, and are higher than the limiting lines of Refs. [10,11], with the only exception of ^{56}Fe. These facts confirm that a strong octupole fragmentation occurs in the nucleus in the mass region of $44<A<60$.

The $\lambda=2$, 3, and 4 total low-lying strengths detected in the examined nuclei are shown in the left part of Fig. 10 as a function of the neutron numbers. The respective observed percentages of the sum rules are also shown in the right part of Fig. 10. The strengths of ^{58}Ni (see crosses in Fig. 10) are generally higher than those of other nuclei. At the neutron closure $N=28$, the Ti and Fe isotopes (see circles and squares in Fig. 10) have the smallest $\lambda=2$ strength and the highest $\lambda=3$ and 4 EWSR fraction.

TABLE II. Energy limits ($E_{\rm lim}$) used in the sum of Eq. (4) for the quoted nuclei.

Nucleus	$E_{\rm lim}$ (MeV)	Reference
^{46}Ti	8.230	[6]
^{48}Ti	8.267	[5]
^{50}Ti	10.495	[4]
^{54}Fe	10.586	[4]
^{56}Fe	8.536	present work
^{48}Ca	13.493	[8]
^{52}Cr	9.440	[4]
^{58}Ni	11.728	[7]

V. MODEL CALCULATIONS OF TRANSITION MATRIX ELEMENTS

In this section, we compare the predictions from the RPA calculations with the ^{54,56}Fe transition matrix elements and their isovector contents.

The $1p$-$1h$ strength distributions and fragmentation are calculated for the measured energy range in a mean-field approach based on single-particle states interacting via pairing in the framework of the BCS approximation plus RPA. Single-particle wave functions and energies were calculated using a simple Woods-Saxon potential given in Table III, for the central and spin-orbit neutron and proton wells. The number of single-particle levels involved and the Fermi energy were adjusted in the BCS procedure so as to reproduce the experimental separation energies within a few percent. The values used are given in Table III.

The levels so obtained were used to perform a quasiparticle RPA calculation in a complete space. The pairing strength was set to be $G=0.19$ both for protons and neu-

TABLE III. Optical model parameters, Fermi energies, and gap parameters used in the RPA calculation described in the text.

Nucleus	r (fm)	a (fm)	V_n (MeV)	V_p (MeV)	$V_{ls,n}$ (MeV)	$V_{ls,p}$ (MeV)	Ef_n (MeV)	Ef_p (MeV)	Δ_n Calc. (MeV)	Δ_n Expt. (MeV)	Δ_p Calc. (MeV)	Δ_p Expt. (MeV)
^{54}Fe	1.25	0.65	49.7	52.2	24.1	25.3	−11.2	−14.9	1.88	1.87	1.53	1.52
^{56}Fe	1.25	0.65	48.6	53.4	23.1	25.3	−8.8	−16.3	1.32	1.37	1.54	1.57

trons; a shift of −0.4 MeV on the proton energies, estimated by assuming constant charge distributions, was included to take into account both the Coulomb repulsion between the two protons in the pairing modes and the attractive interaction between the proton particle and the proton hole in the surface modes [18].

Both an isoscalar and isovector coupling interaction of the form $Kr\ dV/dr$ was used in the RPA calculation. We used a relation of $K_{\rm isov}=0.3\,K_{\rm isosc}$, and with the strength K fitted to reproduce the energy of the lowest state for each multipolarity. The values of K so obtained were within 10% of the self-consistent one for both $\lambda=2$ and 3. Most of the strength was accounted for; the missing strength in the energy-weighted sum rule was less than 1% for the three multipolarities. The final RPA results for the $\lambda=2$, 3, and 4 isoscalar and isovector transition matrix elements of ^{54}Fe and ^{56}Fe are reported with vertical dotted lines in Figs. 6 and 7, respectively.

As expected, the inclusion of only $1p$-$1h$ configurations in RPA calculations does not reproduce the detailed features of the experimental strengths, as can be seen in Figs. 6, 7, and 8. However, the calculations correctly predict a larger fragmentation of the $\lambda=2$ and 3 strengths in ^{54}Fe compared with the case in ^{56}Fe. An analysis of the calculated RPA wave functions amplitudes for these levels (see Table IV) shows that the two additional neutrons in ^{56}Fe above the $f_{7/2}$ shell produce an increase in the transitions involving orbitals above and a decrease in those involving orbital below this shell. This results in a larger collectivity of the 2_1^+ and 3_1^- levels in ^{56}Fe compared with the case in ^{54}Fe. This distribution difference of the strength is rather satisfactory since we do not make any adjustment of the single-particle energies obtained by using a rather general potential. This overall agreement shows that even using a simple interaction, general features can be reproduced. On the other hand, more quasiparticle configurations are needed to act as doorways for strength fragmentation.

TABLE IV. Amplitudes for the 2_1^+, 3_1^-, and 4_1^+ excitations in ^{54,56}Fe evaluated from the RPA calculations described in the text.

Level	Transition	^{54}Fe	^{56}Fe
$J^\pi=2_1^+$	$\pi:(f_{7/2})\rightarrow(f_{7/2})$	0.71	0.46
	$\pi:(f_{7/2})\rightarrow(p_{3/2})$	0.09	0.07
	$\nu:(f_{7/2})\rightarrow(p_{3/2})$	0.11	
	$\nu:(f_{7/2})\rightarrow(f_{7/2})$	0.03	
	$\nu:(p_{3/2})\rightarrow(p_{3/2})$		0.28
	$\nu:(p_{3/2})\rightarrow(p_{1/2})$		0.06
$J^\pi=3_1^-$	$\pi:(d_{3/2})\rightarrow(f_{7/2})$	0.42	0.14
	$\pi:(s_{1/2})\rightarrow(f_{7/2})$	0.14	0.10
	$\pi:(d_{3/2})\rightarrow(p_{3/2})$		0.03
	$\pi:(f_{7/2})\rightarrow(g_{9/2})$	0.08	
	$\nu:(p_{3/2})\rightarrow(g_{9/2})$		0.45
	$\nu:(f_{7/2})\rightarrow(g_{9/2})$	0.10	0.09
$J^\pi=4_1^+$	$\pi:(f_{7/2})\rightarrow(f_{7/2})$	0.92	0.78
	$\pi:(f_{7/2})\rightarrow(p_{3/2})$		0.03
	$\nu:(p_{3/2})\rightarrow(f_{5/2})$		0.05
	$\nu:(f_{7/2})\rightarrow(p_{3/2})$	0.02	0.03
	$\nu:(f_{7/2})\rightarrow(p_{1/2})$		0.02

VI. CONCLUSIONS

The results of the inelastic scattering of deuterons at 56 MeV have been presented for the low-lying states at $E_x=4.4$–8.6 MeV of excitation energy in ^{56}Fe. The energy resolution of 30 keV obtained with the magnetic spectrometer has allowed us to resolve most of the known excited levels of ^{56}Fe, and to evidence new levels at excitation energies greater than 7 MeV. By combining the present data with the data for the levels for excitation energies up to 4.5 MeV given in Ref. [1], discussion on the fragmentation of the transition multipolarities becomes possible.

Experimental cross sections have been described by the coupled-channel calculations in order to make the spin-parity assignment of the observed levels. From these analyses, the isoscalar transition matrix elements $M(E\lambda)$ for excitation of the investigated levels from the ground state have been deduced and compared with those of other nearby nuclei in the $44<A<60$ mass region where the $\lambda=2$, 3, and 4 multipolarities are highly fragmented and the mean fragmentation values increase with the multipolarity.

We find that the fragmentation of the $\lambda=3$ strength in ^{56}Fe is the smallest among the nuclei with the mass of $44<A<60$, and that the $\lambda=2$ and 3 strengths in ^{56}Fe are less fragmented than those in ^{54}Fe.

In order to understand the reason for this phenomenon, we have performed simple $1p$-$1h$ RPA calculations. We can sufficiently reproduce the gross structure of both the isoscalar and isovector components for the quadrupole, octupole, and hexadecapole excitations of ^{54}Fe and ^{56}Fe. Moreover, the $\lambda=2$ and 3 fragmentation in ^{54}Fe is found to be mostly due to the closure of the $\nu f_{7/2}$ shell, while the collectivity of these two multipolarities in ^{56}Fe is restored by the presence of the two neutrons outside the $f_{7/2}$ shell.

Similar phenomena should be present also in the ^{52,54}Cr isotopes. At present, no high-resolution proton or deuteron inelastic scattering experiments on ^{54}Cr are available in the literature.

ACKNOWLEDGMENTS

The authors would like to thank P. F. Bortignon for helpful suggestions on RPA model calculations. One of us (R.D.L.) acknowledges the hospitality received at RCNP during his stay in Osaka. The present work was supported in part by the Ministry of Education, Science, Sports and Culture (Monbusho) under Grant No. 07404012.

[1] R. De Leo, H. Akimune, N. Blasi, I. Daito, Y. Fujita, M. Fujiwara, S. I. Hayakawa, S. Hatori, K. Hosono, H. Ikegami, T. Inomata, I. Katayama, K. Katori, L. Lagamba, S. Micheletti, S. Morinobu, T. Nakagawa, S. Nakayama, A. Narita, T. Noro, R. Perrino, M. Pignanelli, H. Sakaguchi, J. Takamatsu, A. Tamii, K. Tamura, M. Tanaka, A. Terakawa, T. Tohei, M. Tosaki, T. Yamagata, A. Yamagoshi, M. Yosimura, and M. Yosoi, Phys. Rev. C **53**, 2718 (1996).

[2] F. Iachello, Phys. Rev. Lett. **53**, 1427 (1979).

[3] A. Arima and F. Iachello, Ann. Phys. (N.Y.) **111**, 201 (1978).

[4] M. Fujiwara, Y. Fujita, S. Imanishi, S. Morinobu, T. Yamazaki, H. Ikegami, K. Katori, and S. I. Hayakawa, Phys. Rev. C **32**, 830 (1985).

[5] A. Higashi, K. Katori, M. Fujiwara, H. Ikegami, I. Katayama, S. Morinobu, M. Tosaki, S. I. Hayakawa, N. Ikeda, and H. Miyatake, Phys. Rev. C **39**, 1286 (1989).

[6] M. Fujiwara, S. Morinobu, M. Tosaki, H. Ito, I. Katayama, H. Ikegami, S. I. Hayakawa, N. Ikeda, H. Ohsumi, A. Higashi, and K. Katori, Phys. Rev. C **35**, 1257 (1987).

[7] M. Fujiwara, Y. Fujita, I. Katayama, S. Morinobu, T. Yamazaki, H. Ikegami, S. I. Hayakawa, and K. Katori, Phys. Rev. C **37**, 2885 (1988).

[8] Y. Fujita, M. Fujiwara, S. Morinobu, I. Katayama, T. Yamazaki, T. Itahashi, H. Ikegami, and S. I. Hayakawa, Phys. Rev. C **40**, 1595 (1989).

[9] M. Pignanelli, N. Blasi, S. Micheletti, R. De Leo, M. A. Hofstee, J. M. Schippers, S. Y. van der Werf, and M. N. Harakeh, Nucl. Phys. **A519**, 567 (1990).

[10] P. D. Cottle, M. A. Kennedy, and K. A. Stuckey, Phys. Rev. C **42**, 2005 (1990).

[11] N. V. Zamfir, P. D. Cottle, J. L. Johnson, and R. F. Casten, Phys. Rev. C **48**, 1745 (1993).

[12] Y. Fujita, M. Fujiwara, S. Morinobu, T. Yamazaki, T. Itahashi, H. Ikegami, and S. I. Hayakawa, Phys. Rev. C **37**, 45 (1988).

[13] M. Pignanelli, N. Blasi, S. Micheletti, R. De Leo, L. Lagamba, R. Perrino, J. A. Bordewijk, M. A. Hofstee, J. M. Schippers, S. Y. van der Werf, J. Wesseling, and M. N. Harakeh, Nucl. Phys. **A540**, 27 (1992).

[14] H. Ikegami, S. Morinobu, I. Katayama, M. Fujiwara, and S. Yamabe, Nucl. Instrum. Methods **175**, 335 (1981).

[15] L. K. Peker, Nucl. Data Sheets **61**, 189 (1990).

[16] J. Raynal, computer program ECIS88, in Workshop on Applied Theory and Nuclear Model Calculation for Nuclear Technology Applications (JCTP), Trieste, 1988.

[17] R. J. Peterson, Phys. Rev. C **48**, 1128 (1993); D. S. Oakley, M. J. Smithson, S. Mordechai, C. F. Moore, P. A. Seidl, C. L. Morris, G. C. Idzorek, Z. F. Wang, R. Gilman, J. D. Zumbro, H. T. Fortune, S. J. Seestrom-Morris, K. S. Dhuga, and D. L. Watson, *ibid.* **35**, 1392 (1987).

[18] P. F. Bortignon, R. A. Broglia, D. R. Bes, and R. Liotta, Phys. Rep. **30**, 305 (1977).